Electron-energy losses in hemispherical targets

J. Aizpurua, A. Rivacoba, and S. P. Apell*
Departamento de Física de Materiales, Facultad de Química, Universidad del Pais Vasco/Euskal Herriko Unibertsitatea, Apartado 1072, 20080 San Sebastian, Spain
(Received 15 February 1996)

In the framework of classical dielectric theory, the hemispherical geometry is studied. Calculations on surface modes are carried out for isolated Drude-like hemispheres. The convergence of the results with respect to the number of coupled terms in the expressions of the potential is discussed. The electron-energy-loss probability is studied for Al and Ag particles involving this geometry. The surface modes and hence the energy-loss probability are given by coupled expressions, the physical meaning of which is the coupling among multipolar terms, because of the particular geometry. The results obtained here present a good quantitative agreement with experiments in the case of clear surfaces (Ag) and provide a qualitative understanding for the experiments in Al, in terms of the position and impact parameter of the beam. This allows us to set the validity of the dielectric theory for cases that seemed to question it. [S0163-1829(96)02228-X]

I. INTRODUCTION

The development of the scanning transmission electron microscope (STEM) has increased the interest of studying electron-energy loss. A target can be studied in a standard way using a very well-focused fast electron beam 0.5 nm wide and with an energy of 100 keV. Electrons transmitted across the target provide information on a small area of the target. When scanning the target with this beam, a high-resolution image can be obtained. With the help of an analyzer, a transmission electron-energy spectrum can be obtained for every position of the beam. This spectrum depends on the geometry and chemical composition of the target in a spatially localized region. The loss spectrum is divided into core losses and valence losses: core losses are more easy to interpret in terms of atomic excitation and, therefore, are widely used. Valence losses are more intense and provide a large amount of information, which, however, is more of a challenge to interpret, because of the dependence on the geometry, coupling between surfaces, target size, and relative impact parameter. It is possible to study in this way, e.g., oxide layer formation, metallic interfaces, and catalysis phenomena.

Since Ritchie[1] predicted surface excitations, the classical dielectric theory has been largely applied in studying the response of a medium to an incident charge.[2–4] This theory has been developed for planar interfaces by several authors.[5–9] The study of electron-energy losses, in small spherical particles, was first tackled by Fujimoto and Komaki.[10] Schmeits,[11] Kohl,[12] Penn and Apell,[13] among others, applied the free-electron model to study losses in spherical surfaces. Ferrell and Echenique,[14] showed the importance of taking into account the contribution of all multipolar terms, even for electrons not penetrating the target. Dispersion effects have also been taken into account in several works.[15,16] Bausells, Rivacoba, and Echenique[17] studied the case of penetrating trajectories. In most of these works, a classical approximation is used when supposing that the electrons are point particles moving with a constant velocity. The validity and limits of this approximation have been studied by Ritchie[18] and Ritchie and Howie.[19] Echenique, Bausells, and Rivacoba[20] have presented an approach to the problem of interaction between charged particles and surfaces based on the self-energy formalism. In this theory, the beam is represented by a wave function, thus taking into account quantum effects for the probe.

Modes and energy losses in different geometrical systems have been studied by several authors: cylinders,[21–25] spheroids,[26] edges,[27] cubes,[28] two spheres,[29] two cylinders,[30] and the sphere-plane system.[31,32] Many mixed geometries have been studied in the literature trying to adapt theory to experiments. Batson[33,34] observed anomalous excitations in the range of 2–5 eV in oxidized Al spheres that he attributed to the coupling between the spheres. Schmeits and Dambly[29] studied these effects theoretically, considering noninterpenetrating spheres. Similar anomalous loss peaks were reported by Wang and Cowley[31] for Al particles on different substrates, but their theoretical development did not reproduce the correct result in the limiting case of an isolated sphere, raising doubts about their treatment. Howie and Walsh[35] presented results for the case of small Al particles in an AlF_3 matrix and discussed it in terms of dielectric excitation theory for a two-phase medium. Ugarte, Colliex and Trebbia[36] studied oxidized Si particles that presented unexpected surface excitations at 3–4 eV, which they interpreted with the introduction of a second ultrathin layer of Si on top of the oxide layer.

Recently Ouyang, Batson, and Isaacson[37,38] observed an anomalous behavior in the energy-loss peak for Ag hemispherical particles when varying their size. Wang and Cowley[31] observed hemispherical Al particles on a AlF_3 substrate that also presented unexplained peaks. Ouyang *et al.* found a shift down in the electron-energy-loss peak (from 3.6 to 3.1 eV) going from 20-nm particles down to 2 nm in diameter. The behavior of electron-energy-loss spectroscopy (EELS) on particles less than 2 nm agrees with that observed in optical absorption, which has been studied and explained in the framework of the quantum theory.[39,40] Ouyang *et al.* claimed that the shift they observed was also due to quantum size effects, but as we will see below, this effect can be

explained in the framework of the dielectric theory for the range of sizes studied (2–20 nm). These anomalous data make it necessary to study, in a more complete way, the hemispherical geometry that seems to be the most proper theoretical approach to these experiments, in the way that this is the shape that the particles take when they are settled on a plane. In our study, we will calculate the surface modes for a Drude-like hemisphere and in a second step we will study how modes are excited for different target sizes and impact parameters. In this problem, all the multipolar terms in the modes equation are coupled and a cutoff has to be made; therefore, a discussion on the convergence of the modes will be necessary. Results for Ag hemispheres—as used by Ouyang *et al.*—confirm the validity of the dielectric theory at least for particles larger than about 2 nm. The data of Wang and Cowley[31] are explained as well, involving a hemispherical geometry. Using our scheme of space partition, EELS for other geometries as isolated or half-embedded spheres can be successfully reproduced. The expressions used in this paper allow the use of experimental dielectric functions.[41] This makes the results more relevant to experiments. These points, taking into account both the material properties and the geometrical features, are the two main characteristics in our theoretical development.

II. HEMISPHERICAL SURFACE-PLASMON MODES

We will determine the surface-plasmon modes of a hemisphere using the geometry shown in the inset in Fig. 1(a). In order to write the potential ϕ as a regular multipolar expansion, we divide the space into three different parts, the dielectric functions of which are ε_1, ε_2, and ε_3, respectively. Then the potential in each medium can be written as the appropriate multipolar expansion.

In the following, we will treat a metallic hemisphere in vacuum, i.e., $\varepsilon_1=\varepsilon_3=1$ and $\varepsilon_2\equiv\varepsilon=1-\omega_p^2/\omega^2$, a Drude dielectric function, in order to get well-defined surface modes of the hemispherical geometry in the case of a metal with bulk-plasmon frequency ω_p.

The expressions of the potential are

$$\phi_1(\mathbf{r},\omega)=\sum_{l=0}^{\infty}\sum_{m=-l}^{l} A_{lm}\,\frac{a}{r^{l+1}}\,P_m(\mu)e^{im\varphi} \qquad \text{for} \quad r\geqslant a,$$

$$\phi_2(\mathbf{r},\omega)=\sum_{l=0}^{\infty}\sum_{m=-l}^{l} B_{lm}\,\frac{r^l}{a^{l+1}}\,P_{lm}(\mu)e^{im\varphi}$$

$$\text{for} \quad r\geqslant a, \quad 0\leqslant\theta\leqslant\pi/2,$$

$$\phi_3(\mathbf{r},\omega)=\sum_{l=0}^{\infty}\sum_{m=-l}^{l} C_{lm}\,\frac{r^l}{a^{l+1}}\,P_{lm}(\mu)e^{im\varphi}$$

$$\text{for} \quad r\leqslant a, \quad \pi/2\leqslant\theta\leqslant\pi, \tag{1}$$

where $\mu=\cos\theta$, a is the radius of the hemisphere, $(r,\ \theta,\ \varphi)$ are the standard spherical coordinates, and $P_{lm}(\mu)$ are the Legendre functions. The coefficients A_{lm}, B_{lm}, and C_{lm} are obtained from the continuity of the potential and the normal component of the displacement field on the surfaces between two different media.

The continuity between media 2 and 3 yields

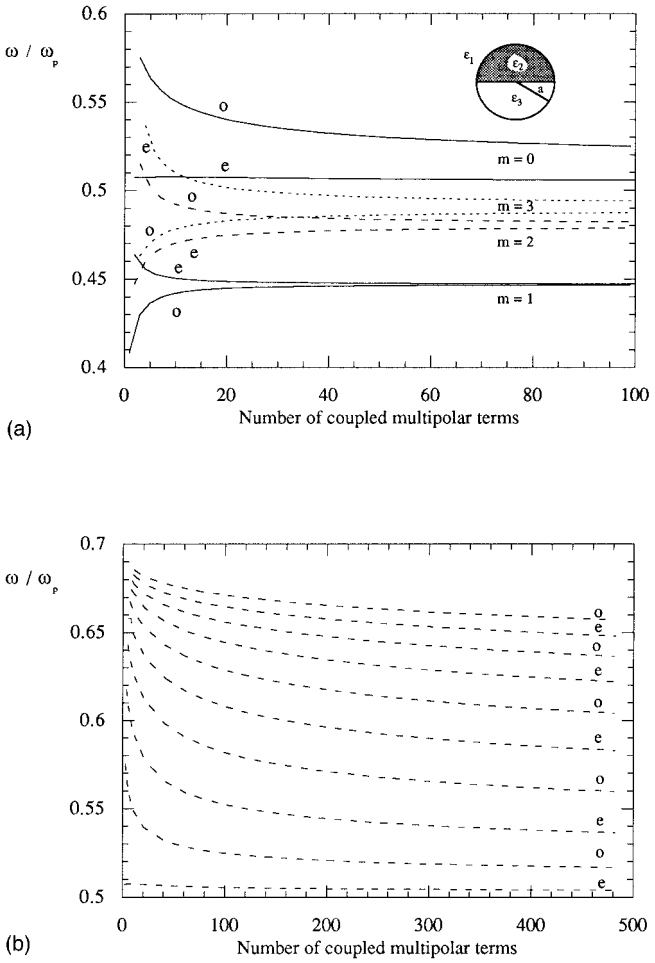

FIG. 1. (a) Lowest m-mode spectrum for a hemisphere when increasing the number of coupled terms (j max), that is the number of equations to find the interacting modes. Two different ways of convergence can be seen for an even (e) or an odd (o) maximum number of equations. The pace partition for calculating the hemispherical surface modes is shown in the insert. In our particular case, media 1 and 3 are vacuum ($\varepsilon_1=\varepsilon_3=1$) and medium 2 is a Drude-like metal with $\omega_p=15.1$ eV and damping $\gamma=0.02\omega_p$. a is the radius of the hemisphere. ω is expressed in units of ω_p. (b) As in (a) for the first five $m=0$ modes with an even (e) or an odd (o) maximum number of equations.

$$C_{lm}=\eta_{lm}B_{lm}, \quad \text{where} \quad \eta_{lm}=\begin{cases}1, & l+m \quad \text{even}\\ \epsilon, & l+m \quad \text{odd}.\end{cases} \tag{2}$$

The angular dependence of the expressions in the potential can be reduced by projecting over the spherical harmonic $(\alpha P_{jm}(\mu)e^{im\varphi})$, and then integrating over the hemisphere. Because of the orthogonality of the set $e^{\mathrm{im}\varphi}$ on the hemisphere, only the mth term remains. Wang and Cowley[31] calculated hemispherical modes, but they only took into account $m=0$ modes. The importance of modes with $m\neq0$ will be discussed below. The $P_{jm}(\mu)$ set is not orthogonal in the interval (0,1), therefore the continuity between media 1 and 2 and 1 and 3, respectively, together with relation (2) lead to a set of j linear algebraic equations that couples the B_{lm} coefficients for each value of m:

$$\sum_{l=m} N_{jl}^{(m)}(\omega)B_l^{(m)}=0, \tag{3}$$

where $N_{jl}^{(m)}(\omega)$ is the matrix,

$$N_{jl}^{(m)}(\omega)=[\varepsilon l+l\,\eta_{lm}(-1)^{l+j}+(j+1)+(j+1)\,\eta_{lm}(-1)^{l+j}]M_{lj}^{m}, \quad (4)$$

and $B_l^{(m)}$ is the vector, the components of which are the coefficients B_{lm}, M_{lj}^{m} is given by

$$M_{lj}^{m}=\int_0^1 P_l^m(\mu)P_j^m(\mu)d\mu. \quad (5)$$

For $l+j$ odd, the integrals must be numerically computed, while for $l+j$ even numerical values can be found in the literature.[42] Then they become $M_{lj}^{m}=[\delta_{lj}(2l+1)][(l+m)!/(l-m)!]$, where δ_{lj} is the Kronecker δ. This means that only terms with different parity are coupled, except for the case of the last term where $l=j=j$ max, which can present the same parity.

The values of $\omega(=\omega_m)$ that satisfy Eq. (3) are the m modes of the hemispherical geometry. This infinite set of linear algebraic equations will have a nontrivial solution, $\phi\neq 0$ (that is all the coefficients B_{lm} nonzero), only if the system matrix determinant is equal to zero, viz.,

$$\det[\mathbf{N}^{(m)}(\omega)]=0. \quad (6)$$

We obtain this coupled expression for the l coefficients, because of the asymmetry of the problem (hemisphere). If we had considered a full sphere, we would have a δ_{lj} factor instead of M_{lj}^{m}. The coupling does not allow us to talk about l modes for this hemispherical geometry, but rather we have to talk about coupled modes. The only index corresponding to a conserved symmetry that we can give these modes is the azimuthal m value. We have to take into account the fact that the equation system is infinite and then the number of equations j have to be truncated at a maximum j (j max) for every m in order to solve the linear system. This j max corresponds to neglecting j-polar terms with $j>j$ max in the potential. Equation (6) reduces to calculate the zeros of a polynomial in ω^2 of order j max-m.

We examine, in Fig. 1(a), the solution of Eq. (3) for the energy of the lowest coupled modes, for different values of m, as a function of the number of coupling equations, i.e., j max. Two features should be pointed out when analyzing the convergence of the modes frequencies. The first is the different way in which convergence is achieved when terminating the set of equations by even or odd j max values. The different behavior of the solutions depending on the parity of j max$+m$, can be explained in terms of the pattern of their corresponding charge density. Notice that terms with odd $l+m$ pile charge up at the bottom of the hemisphere ($\mu=0$), while those corresponding to even $l+m$ do not. We have already seen in Eq. (3) that the jth multipolar term couples to other terms of different parity, except in the case of the last term where $l=j=j$ max, therefore, the coupling between terms presents a different physical behavior, depending on the parity of the last term that we consider, as it can be observed in Fig. 1(a).

The second feature is the fact that it is necessary to use a very large number of equations to ensure good convergence. It can be seen in Fig. 1(a) that there is a spectrum of modes approaching $0.45\omega_p$ for $m=1$, $0.48\omega_p$ for $m=2$, $0.49\omega_p$ for $m=3$, and 0.51–$0.52\omega_p$ for $m=0$. Notice that the mode labeled as $m=1$ presents the faster convergence behavior. These are interesting modes to test in experiments, since they differ in frequency from those in other geometries such as the spherical one for which the first surface mode ($l=1$) occurs at $\omega=\omega_p/\sqrt{3}\cong 0.57\omega_p$. The slow convergence of the mode frequencies is basically due to the fact that spherical harmonics are not an ideal basis for describing geometries that contain sharp surfaces (Gibb's phenomenon[43]), as in the case of the hemispherical geometry. Nevertheless, the problem can be solved by taking into account a large enough number of equations, as shown in Fig. 1(a). It is evident from Eq. (4) that the positions of the modes, being solutions of Laplace's equation, which has no intrinsic length scale, do not depend on the radius of the particle. However, the strength of the different modes will depend on the particular circumstances of excitation (radius, impact parameter, etc.).

In addition to the modes presented in Fig. 1(a), there are higher modes for each m value. In Fig. 1(b), we plot the lowest five solutions for $m=0$, where one can see a clear difference in the value for modes with even or odd j max. Opposite to the case of the first modes in Fig. 1(a), here branches corresponding to even and odd j max do not seem to converge to a single value. This is connected to the different way of coupling of the M_{lj}^{m} terms and, therefore, the different scheme of piling up charge on the bottom of the hemisphere. The charge density of the $m=0$ mode has no azimuthal dependence, so it is distributed over the whole hemispherical surface and bottom through the l coupling. Because of this distribution, the parity of the last l coupled term in this case will become crucial in the charge distribution and in convergence of solutions. Although one cannot properly speak about $m=0$ modes, because of the problems with the convergence, the limits and physical meaning of these upper solutions will be discussed when studying the spectra of losses. In modes where $m\neq 0$, the charge density oscillation is proportional to $\cos m\varphi$ over the hemispherical surface, for example, the dipolarlike mode corresponding to $m=1$. The fact that the $m=0$ mode has a higher value than some of the other modes ($m=1$ and 2) is as well associated with its peculiar charge-density distribution. On the other hand, the larger the number of coupled multipolar terms is, the more new upper solutions appear closer to ω_s (planar surface plasmon). The mechanism to recover planar excitations is, in that way, the piling of modes around ω_s that can be excited by the particular circumstances of the trajectory, as we will see in the next section.

III. ELECTRON-ENERGY LOSSES IN HEMISPHERICAL PARTICLES

We will, in this section, show the validity of the dielectric theory for large enough objects by comparing the predicted energy losses with those of the experiments in Refs. 31 and 38, respectively. The formalism—presented here to give a general overview—has already been used in other geometries[44] and consists in evaluating the screened interaction for particle positions all along the trajectory. This

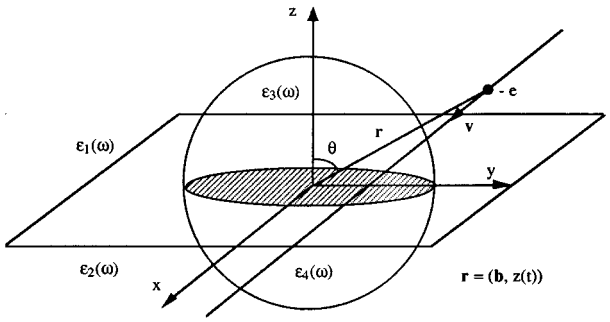

FIG. 2. Space division for calculating the energy-loss spectrum for an electron passing a ''spherical object'' embedded in a surface. Four different media are used in the calculations. Spherical coordinates are used to describe either the media or the electron trajectory. **b** is the impact parameter.

screened interaction is calculated by making use of the standard continuity conditions. The dynamic features of the problem are taken into account by multiplying the interaction by the charge density of the probe and integrating over the trajectory. In this way, the probability of losing energy $\hbar\omega$ for an electron traveling with velocity v, as shown in Fig. 2, is in atomic units:[32]

$$P(\omega)=\frac{1}{\pi}\int_{-\infty}^{+\infty}d\mathbf{r}'\int_{-\infty}^{+\infty}d\mathbf{r}\ \mathrm{Im}\{\rho^*(\mathbf{r},\omega)W^{\mathrm{ind}}(\mathbf{r},\mathbf{r}',\omega)\times\rho(\mathbf{r}',\omega)\},\tag{7}$$

where $\rho^*(\mathbf{r},\omega)$ is the Fourier transform of the charge density and $W^{\mathrm{ind}}(\mathbf{r},\mathbf{r}',\omega)$ is the ω component of the screened interaction at $\mathbf{r}$ caused by a charge at $\mathbf{r}'$.

This expression can be obtained both in a self-energy formalism[44] and in a classical treatment.[32] The connection between a classical and a quantal treatment was already pointed out by Ritchie and Howie.[18,19] In Eq. (7), retardation is not taken into account, but this is supposed to be a good approximation if the electron travels close enough to the target and if the target is $\leqslant$30 nm. Recoil is also not taken into account, because of the high velocity of electrons considered (100 keV).

In order to write the screened interaction in a hemispherical geometry, we divide the space into four different parts characterized by their local dielectric functions $\varepsilon_1(\omega)$, $\varepsilon_2(\omega)$, $\varepsilon_3(\omega)$, and $\varepsilon_4(\omega)$, respectively, as shown in Fig. 2. This space partition allows us to recover the already studied geometrical compositions, such as a sphere or an embedded sphere.

We have calculated the screened interaction $W(\mathbf{r},\mathbf{r}',\omega)$ in this geometry. We write it in spherical coordinates as a proper multipolar expansion in every medium. We show first the case of nonpenetrating trajectories ($r'>a$), that is the electron traveling in the medium labeled 1 all the time. The generalization for penetrating trajectories can be performed in a straightforward way. Following Zaremba,[45] we write the plane image potential separately. Then we have

$$W_1(\mathbf{r},\mathbf{r}',\omega)=\frac{1}{\varepsilon_1}\frac{1}{|\mathbf{r}-\mathbf{r}'|}+\frac{1}{\varepsilon_1}\frac{\varepsilon_1-\varepsilon_2}{\varepsilon_1+\varepsilon_2}\frac{1}{|\mathbf{r}-\mathbf{r}''|}+\sum_{l=0}^{\infty}\sum_{m=-l}^{l}A_{lm}(r',\mu')\frac{a^l}{r^{l+1}}P_{lm}(\mu)e^{\mathrm{i}m(\varphi-\varphi')}\quad\begin{pmatrix} r\geqslant a\\ 0\leqslant\theta\leqslant\pi/2\end{pmatrix},$$

$$W_2(\mathbf{r},\mathbf{r}',\omega)=\frac{2}{\varepsilon_1+\varepsilon_2}\frac{1}{|\mathbf{r}-\mathbf{r}'|}+\sum_{l=0}^{\infty}\sum_{m=-l}^{l}B_{lm}(r',\mu')\frac{a^l}{r^{l+1}}P_{lm}(\mu)e^{\mathrm{i}m(\varphi-\varphi')}\quad\begin{pmatrix} r\geqslant a\\ \pi/2\leqslant\theta\leqslant\pi\end{pmatrix},$$

$$W_3(\mathbf{r},\mathbf{r}',\omega)=\sum_{l=0}^{\infty}\sum_{m=-l}^{l}C_{lm}(r',\mu')\frac{r^l}{a^{l+1}}P_{lm}(\mu)e^{\mathrm{i}m(\varphi-\varphi')}\quad\begin{pmatrix} r\leqslant a\\ 0\leqslant\theta\leqslant\pi/2\end{pmatrix},$$

$$W_4(\mathbf{r},\mathbf{r}',\omega)=\sum_{l=0}^{\infty}\sum_{m=-l}^{l}D_{lm}(r',\mu')\frac{r^l}{a^{l+1}}P_{lm}(\mu)e^{\mathrm{i}m(\varphi-\varphi')}\quad\begin{pmatrix} r\leqslant a\\ \pi/2\leqslant\theta\leqslant\pi\end{pmatrix}.\tag{8}$$

The direct Coulomb term (in W_1) and the planar ones (in W_1 and W_2) can be expressed as multipolar expansions too. We have to calculate the $A_{lm}(r',\mu')$ coefficients in order to get the complete interaction in medium 1. These coefficients will be given by an infinite set of coupled equations, as in the case of the modes in Eq. (3), but now we will have more coefficients coupled to $A_{lm}(r',\mu')$, because we are working with a space divided into four parts. After using the continuity of the interaction and its derivative normal to the surface at every interface, we get the following set of equations:

$$\sum_{l=m}^{\infty}[1+\xi_{lm}(-1)^{l+j}]M_{lj}^{m}C_{lm}(r',\mu')-\sum_{l=m}^{\infty}[1+\eta_{lm}(-1)^{l+j}]M_{lj}^{m}A_{lm}(r',\mu')=\sum_{l=m}^{\infty}\left[\frac{2}{\eta_{lm}(\varepsilon_1+\varepsilon_2)}+\frac{2}{\varepsilon_1+\varepsilon_2}(-1)^{l+j}\right]d_{lm}\left(\frac{a}{r'}\right)^{l+1}\times P_{lm}(\mu')M_{lj}^{m}\tag{9}$$

and

$$\sum_{l=m}^{\infty}[1+\xi_{lm}(-1)^{l+j}]lM_{lj}^{m}C_{lm}(r',\mu')$$

$$+\sum_{l=m}^{\infty}\left[\frac{\varepsilon_1}{\varepsilon_3}+\frac{\varepsilon_2}{\varepsilon_4}\,\eta_{lm}(-1)^{l+j}\right](l+1)M_{lj}^{m}A_{lm}(r',\mu')$$

$$=\sum_{l=m}^{\infty}\left[\frac{2\varepsilon_1}{\eta_{lm}(\varepsilon_1+\varepsilon_2)\varepsilon_3}+\frac{2\varepsilon_2}{(\varepsilon_1+\varepsilon_2)\varepsilon_4}\right.$$

$$\left.\times(-1)^{l+j}\right]d_{lm}l\left(\frac{a}{r'}\right)^{l+1}P_{lm}(\mu')M_{lj}^{m}, \tag{10}$$

$$\eta_{lm}=\begin{cases}1, & l+m \text{ even}\\ \varepsilon_1/\varepsilon_2, & l+m \text{ odd},\end{cases}$$

$$\xi_{lm}=\begin{cases}1, & l+m \text{ even}\\ \varepsilon_3/\varepsilon_4, & l+m \text{ odd},\end{cases} \tag{11}$$

where $d_{lm}\equiv(l-m)!/(l+m)!$ and M_{lj}^{m} is defined in Eq. (5).

Equations (9) and (10) constitute a twofold infinite set of linear algebraic equations in the variable C_{lm} and A_{lm}. In order to solve this problem—as in the case of the modes' equation (3)—this system has to be truncated at a maximum j (j max). We will discuss the convergence of the results below. Once the coefficients A_{lm} are calculated, it is possible to evaluate the energy loss probability by using the expression of the screened interaction in (8). We assume a classical electron, moving along the X axis with velocity v as the one in Fig. 2. In this case, the charge density $\rho(\mathbf{r},\omega)$ is given by

$$\rho(\mathbf{r},\omega)=\frac{1}{v}\,\delta(y-b_y)\,\delta(z-b_z)e^{-i\omega x/v}, \tag{12}$$

where b_y and b_z are the coordinates of the impact parameter $b=\sqrt{b_y^2+b_z^2}$.

This yields

$$P(\omega)=\frac{1}{\pi v^2}\int_{-\infty}^{+\infty}dx'\int_{-\infty}^{+\infty}dx\sum_{l=0}^{\infty}\sum_{m=-l}^{l}\frac{a^I}{r^{l+1}}$$

$$\times P_{lm}(\mu)e^{\mathrm{im}(\varphi-\varphi')}\mathrm{Im}\{A_{lm}(\mathbf{r}',\omega)\times e^{-i\omega(x-x')/v}\}, \tag{13}$$

with $r=\sqrt{x^2+b_y^2+b_z^2}$, $\mu=b_z/r$, and $\varphi=\mathrm{arctg}(x/b_y)$.

In the same way that the hemispherical modes were calculated, we now have to study the convergence of the spectra given by Eq. (13). It is convenient to realize that two limits are imposed when solving this problem. First, an upper j for the number of coupled terms in Eqs. (9) and (10), and secondly an upper l that controls the number of multipolar terms, which contribute significantly to the value of $W(\mathbf{r},\mathbf{r}',\omega)$. After having examined many spectra, we have found that the important cutoff is the number of coupled equations (j max) that sets the value of the coefficients. Once these coefficients are solved, it is not as important to use a large number of them, because the large l values do not change the spectrum noticeably. It is enough to consider the contribution of the 20 first multipolar terms for values of the radius about 15 nm in aluminum.

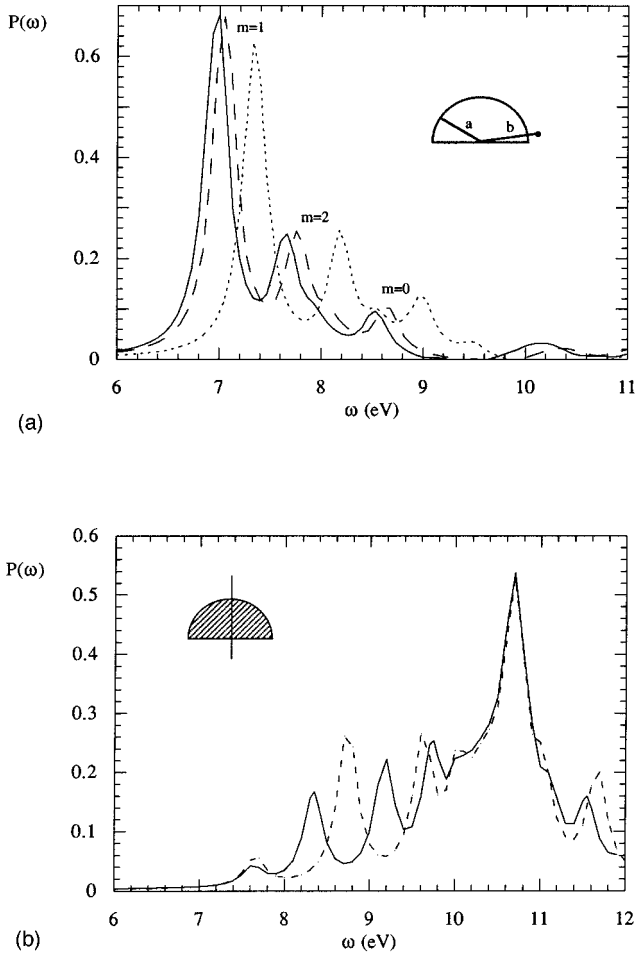

FIG. 3. (a) Energy-loss probability $P(\omega)$ for an Al Drude hemisphere of radius $a=10$ nm when the incident electron passes near the edge of the hemisphere ($b=11$ nm). The convergence of the solution is shown when limiting the number of coupled equations (j max) to 20 (dotted line), 100 (dashed line), and 200 (solid line). (b) Energy-loss probability $P(\omega)$ for an Al Drude hemisphere of radius $a=10$ nm when the trajectory of the electron is axial. 20 terms (dashed line) and 100 terms (solid line) are used in calculations. In both cases, $\omega_p=15.1$ eV and $\gamma=0.02\omega_p$.

In Fig. 3(a), a loss spectrum for an Al (Drude) hemisphere is shown. We have taken $\omega_p=15.1$ eV and used a Drude damping γ, such that $\gamma=0.02\omega_p$. The radius of the hemisphere is 10 nm and the electron travels close to the corner, 1 nm outside of it parallel to the hemisphere base. We find that it is necessary to use at least 100 (j max) equations (dashed line) to ensure reasonable convergence. There appears an excitation around 7 eV ($0.46\omega_p$), which basically corresponds to the hemispherical mode $m=1$ that we have calculated in the previous section. The small shift in the $m=1$ mode energy is due to the damping that we are using. The various modes of excitation have charge densities proportional to $\cos m\varphi$, which in the case of $m=1$ corresponds to a dipolarlike charge distribution in the azimuthal angle, that is a positive charge in one half of the hemisphere and a negative one in the other. The smaller peaks are related to modes with $m=0$ and 2, the $m=0$ mode coming from one of the upper solutions that can be seen in Fig. 1(b). The position of these peaks depends strongly on the number of coupled

terms that are considered (as well as on the parity of the last term), as found in the case of the upper modes. Because of the instability of these modes, one cannot be sure whether they represent real excitations of the target or are merely spurious peaks due to the limitations of the mathematical approach. Nevertheless, the peak labeled as $m=2$ maintains a constant height, while its energy shifts down and approaches a fixed value, in agreement with the corresponding tendency of the upper modes. In the case of the peak labeled as $m=0$, we observe that its height decreases with an increasing number of terms in Eqs. (9) and (10). This mode ($m=0$) is the most problematic and we tend to think that it is a spurious peak, because of the relatively poor convergence.

In order to establish the suitability of our approach, we calculate in Fig. 3(b) the energy loss for an axial trajectory, which can only excite $m=0$ modes, which is the most unfavorable situation, as we have seen (we use 20 and 100 terms in calculations). The size and characteristics of the target are the same as in Fig. 3(a). The screened interaction has been calculated taking into account the penetrating trajectory in a similar way to the previous spectrum. One can recognize the similarity between the spectrum of losses, and the spread of modes around the ω_s value that we talked about in the previous section [see Fig. 1(b)]. A dominating peak is observed in 10.7 eV, that is the planar surface mode frequency, which is recovered through the l coupling for $m=0$, because of the accumulation of modes close to ω_s. For this beam position, the geometry of the target does not differ very much from that of a film or even from that of a sphere, since the corners are far away from the trajectory and then their influence on the spectrum is small. Echenique and co-workers[46] proved that, in the limit of very large spheres, the energy loss experienced by a fast probe could be interpreted in terms of the stopping power of a particle moving near a planar surface at an instantaneous impact parameter. We find in Fig. 3(b) that the stability of the solution is quite good around the dominant peak at ω_s. The other neighboring peaks concide with some of the solutions that we calculated in Fig. 1(b), but they are unstable with a behavior similar to that discussed in the previous spectrum. In spite of the slow convergence, it is clear from these figures the validity of the spectra obtained and that it is necessary to use at least 100 terms in the calculations in order to obtain convergent results.

The formalism used here allows us to use experimental dielectric functions, which allows for a more realistic description of the target excitation. In general, a much better convergence of the multipolar series is obtained and no instability appears for such a dielectric response function. In Fig. 4, we compare the spectra for an aluminium hemisphere, as obtained with the experimental $\varepsilon(\omega)$ (Ref. 41) when the electron passes close to the top of the target and close to the corner. For an electron passing close to the top, the spectrum is similar to the one of an isolated sphere, showing the typical 8.9 and 9.7-eV spherical excitations for $l=1$ and 2. These spherical peaks are excited via the piling up of modes around these values, as mentioned before. Notice, however, the difference in strength. Using experimental values or a Drude ε gives a small shift of 0.3 eV and a different absolute weight in excitations, but the qualitative behavior is the same, as can be seen by comparing Figs. 3(a) (dashed) and line B in Fig. 4. When the electron travels close to the corner of the hemisphere, there appears an excitation that does not correspond to the spherical shape (line C), as we have mentioned above. This excitation appears for the top situation too, but with a much weaker spectral strength, which is in agreement with the impact parameter dependence for Al particles in the results of Wang and Cowley.[31] This is the basis for our referring to this excitation as a hemispherical surface plasmon.

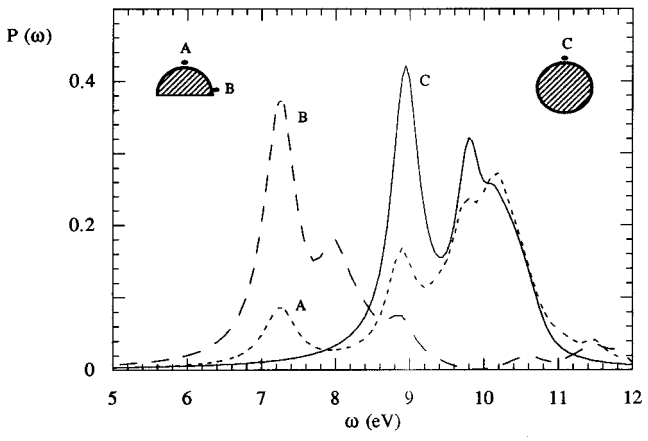

FIG. 4. Energy-loss probability $P(\omega)$ for Al hemispherical targets of radius $a=10$ nm. In both cases, the electron travels 1 nm from the surface parallel to the planar surface. The solid line (C) shows the spectrum for an isolated Al sphere, whereas short dashed (A) and dashed (B) lines show the spectra for an electron traveling close to the top and the edge of the hemisphere, respectively. Notice that B can define the signature of a hemisphere in the same sense as the Mie mode at 9 eV for the sphere.

Ouyang, Batson, and Isaacson[38] obtained high resolution spectra (0.1 eV) for Ag targets that presented an anomalous behavior when varying the size of the samples, as shown in Fig. 5(a). The targets are hemispherical Ag particles that lie on a carbon substrate. These experiments present several advantages, because of the clean surface typical of silver particles, with no oxide layer, and no contamination on the surface. A rough estimation of the C support effect can be performed by assuming that the lower half space consists of C. One can conclude that the C support effect is not very relevant to the spectra in this energy range: the spectra are shifted 0.1 or 0.2 eV down and peaks are broader than those corresponding to the isolated hemisphere. The dependence of the loss spectra on both the particle size and beam position can be well understood, in this way, in terms of the spectra corresponding to an isolated hemisphere. The convergence in this problem is less difficult and has been commented on above, so we do not discuss it for Ag particles. Anyway, we always use a large enough number of terms in the calculations. We will solve the set of Eqs. (9) and (10) for (see Fig. 2) $\varepsilon_1=\varepsilon_2=\varepsilon_4=1$ and $\varepsilon_3=\varepsilon$ (experimental Ag).[41] The use of other optical data[47] can shift the spectra a few tenths of eV. Figures 5(b) and 5(d) show the spectra of Ag hemispheres for two different sizes, 5 and 40 nm, respectively. It can be seen that two dominating excitations appear depending on the position of the electron. In all cases, electrons passing close to the top of the particle present an excitation at 3.6 eV, whereas electrons passing close to the corner present an excitation at 3.2 eV. As we increase the size of the sample, the top excitation (3.6 eV) is more important in weight than the

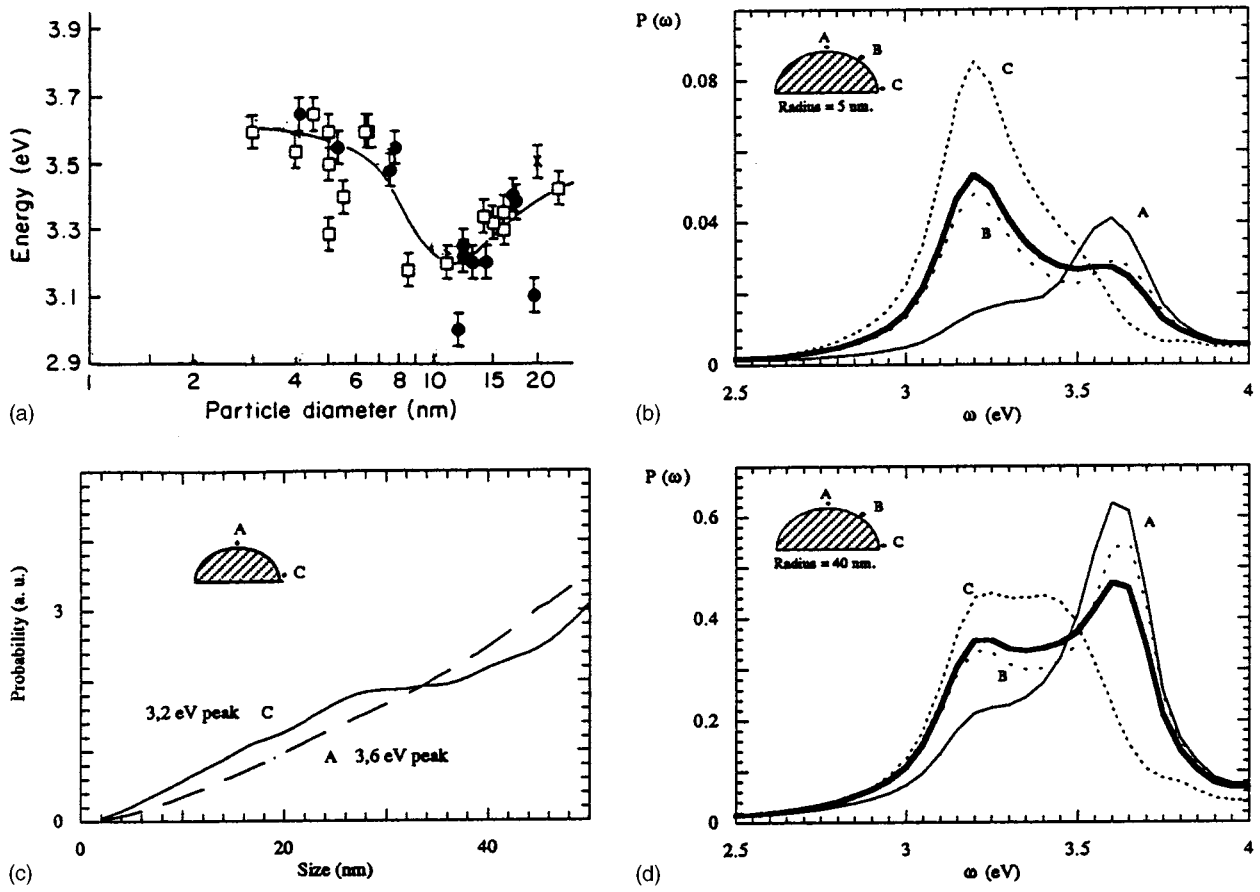

FIG. 5. To the right (b) and (d) energy-loss spectra $P(\omega)$ for Ag hemispheres when varying the radius ($a=5$ and 40 nm, respectively) for three different trajectories (A: $\theta=0°$, B: $\theta=45°$, and C: $\theta=85°$) of the electron. The thick line is the average of three trajectories. To the left (a) and (c) experimental points by Ouyang *et al.*, as in Fig. 3 of Ref. 38 and the integrated energy-loss probability $P(\omega)$ of the 3.6- and 3.2-eV loss peaks in Ag hemispherical particles for the A and C positions of the beam, respectively, to the right. 100 terms have been used in calculations.

lower one, as Ouyang *et al.* observed in their experiments in the range of 2–20 nm. Both excitation modes are present for every size, but they are finally excited depending on the position of the beam and with a different relative weight depending on the size itself. This gives the increasing tendency from 3.2 to 3.6 eV. Mode frequencies are independent of the radius and impact parameter, but not the coupling strength, the weight of which will be given mainly by these particular parameters. This is why there appear both excitations in the experimental curve in such a narrow size range. The evolution of the excitation probability of the 3.2 and 3.6 eV peaks for the C and A positions of the beam, respectively, is shown in Fig. 5(c). The dominating peak changes from C to A when increasing the particle size. The 3.6-eV peak (A) increases its excitation probability with size in a monotonous way [Fig. 5(c)], whereas the strength of the 3.2-eV peak (C) goes down and broadens out when the particle size is about 30 nm. The lower excitation (C) starts spreading upwards in energy, as seen in Fig. 5(d) for a 40-nm particle, and hence the excitation probability flattens out in this size range for the 3.2-eV excitation [Fig. 5(c)]. In this way, the cause of the change from 3.2 to 3.6 eV is most likely due to the spreading up of excitation modes in the lower peak for a defined size of the particle.

In the same way as it has been shown above for nonpenetrating trajectories, penetrating trajectories have been studied to compare, in a more realistic way, theory to experiments. Similar conclusions can be inferred in this case with a little shift down from 3.2 to 3.1 eV in the bottom excitation. In Fig. 6, integrated energy loss probability versus impact parameter b is shown for a 5-nm Ag particle at the edge excitation (3.1 eV) and the top one (3.6 eV). For bigger particles, a spread towards spherical and planar surface excitations will take place. When the electron penetrates the particle, the closer to the edge of the hemisphere the electron travels, the higher the 3.1-eV excitation is, whereas the 3.6-eV excitation peak keeps its strength almost unchanged inside. For nonpenetrating trajectories, the edge excitation is stronger in weight than the top one. This can explain why there is such a strong spread of excitations in such a short size range in Ouyang's experimental results. Although the 3.6-eV peak seems to be connected to bulk losses, because of the shape of the curves (almost constant for penetrating trajectories and quickly decreasing for external ones), the main contribution to losses in this peak is due to surface losses. The bulk term has been directly calculated from the direct Coulomb term in the screened interaction $W(\mathbf{r},\mathbf{r}',\omega)$ and its

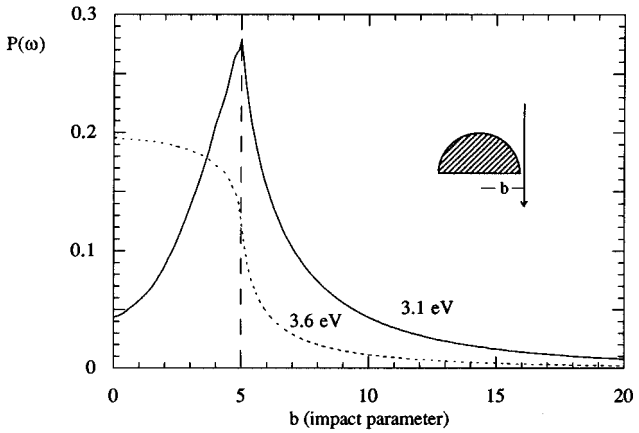

FIG. 6. Energy-loss probability $P(\omega)$ versus impact parameter b at 3.1 and 3.6 eV for hemispherical Ag particles with radius $a=5$ nm. Electron trajectories are as shown in the figure.

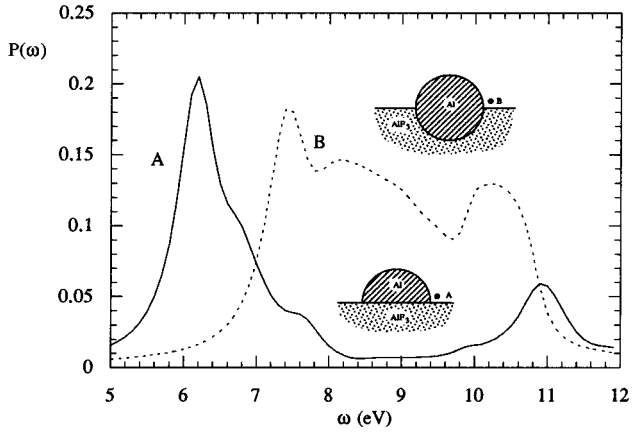

FIG. 7. Energy-loss spectrum $P(\omega)$ for an Al hemisphere on AlF_3 (A) and an Al sphere embedded in AlF_3 (B) of radius $a=10$ nm for the electron trajectory, as shown in the figure.

effect is just to shift the curve a little bit upwards for penetrating trajectories, but not to change the functional dependency. Hence, we can say that the 3.6-eV losses are connected to spherical or quasiplanar surface losses, while the 3.1-eV ones are connected to edge surface losses. Both surface excitations are present at the same time, but it is easier to excite one or the other, depending of the size of the particle and the beam position itself. When we increase the particles' size, we are more likely to excite the top mode (3.6 eV) and this is the tendency observed by Ouyang *et al.*

In other theoretical approaches to the problem of STEM electrons interacting with small particles,[14,26] spherical or spheroidal shapes were studied and electrons could, therefore, not excite other modes other than the spherical or spheroidal ones. Ouyang *et al.*[38] introduced quantum size effects to explain the shift in the 2–20-nm range but, as we have shown, it is not necessary when using a better geometrical description. However, it should be necessary to introduce quantum size effects when studying particles less than about 2 nm.

Wang and Cowley[31] have also presented data involving hemispherical particles. They observed a shift of 3 eV (from 8 to 11 eV) when changing the shape of Al particles over an AlF_3 substrate. This shift can be observed in the loss probability when solving the set of Eqs. (9) and (10) for $\varepsilon_1=1$, $\varepsilon_2=\varepsilon_{AlF_3}$, $\varepsilon_3=\varepsilon_{Al}$, and $\varepsilon_4=\varepsilon_{Al}$ for an embedded sphere or $\varepsilon_4=\varepsilon_{AlF_3}$ for the hemispherical case. In Fig. 7, the spectra for these two cases are shown. It can be seen how the 8-eV peak (B) shifts up to 11 eV (A) as in the experiments and another low-energy peak appears at 6 eV. In order to test a more realistic case, we should introduce an oxide layer covering the Al particle, but it is known[36] that the effect of this is typically to shift the low excitation down about 1 or 2 eV. We could try to reproduce this layer by making medium 1 to be Al_2O_3. When doing this, the 6-eV excitation shifts down, corresponding to the 4.5 eV observed in experiments.[31] In these experiments, the agreement is more qualitative, due to the resolution (1 eV) and that we have not included the oxide layer of aluminum. But as was pointed out by Wang and Cowley,[31] the importance of an accurate geometrical treatment in studying surface excitations is clear, as both our examples show.

IV. CONCLUSIONS

In this paper, we have studied surface-plasmon excitation in a hemispherical geometry, using a macroscopic dielectric formalism. The various modes can be labeled by means of an azimuthal number m and we have discussed the meaning of these modes in terms of the charge density associated with them. As an application of the theory, we have studied the spectra of charged particles, which follow specific trajectories relative to the target. We find that the spectra exhibit additional peaks at energies lower than those corresponding to the sphere modes. When the electron travels close to the edge of the hemisphere, a dipolar excitation ($m=1$) is activated at low frequency corresponding to one of the modes obtained. These modes also contain planar excitations through the l coupling for determined trajectories and large enough targets. In order to obtain spectra as realistic as possible and to facilitate a comparison with experiment, we have used the experimentally determined $\varepsilon(\omega)$. In this way, we have been able to explain the experimental results about the relation between the excitation energy and size in hemispherical Ag particles in terms of the beam position and a more suitable geometrical description. We have also discussed Al particles on an AlF_3 substrate. In neither case was it necessary to introduce a microscopic description of the electronic response. A classical dielectric theory seems capable of explaining most of the geometry-dependent behavior of hemispherical particles larger than 2 nm.

ACKNOWLEDGMENTS

The authors wish to acknowledge Professors A. Howie and P. M. Echenique for their helpful reading of the manuscript and valuable suggestions and Professor Isaacson for his kind permission to reproduce the experimental data in Fig. 5(a) (Ref. 38). They also thank the Basque Country Government-Eusko Jaurlaritza (Project No. PI95/35) and the Swedish Natural Science Research Council for financial support. One of us (J.A.) thanks the 'Hezkuntza, Unibertsitate eta Ikerketa Saila' for their support.

*Permanent address: Department of Applied Physics, Chalmers University of Technology and Göteborg University, S-41296 Göteborg, Sweden.
[1] R. H. Ritchie, Phys. Rev. **106**, 874 (1957).
[2] L. D. Marks, Solid State Commun. **34**, 477 (1980).
[3] R. Nuñez, P. M. Echenique, and R. H. Ritchie, J. Phys. C **13**, 4229 (1980).
[4] A. Howie, Ultramicroscopy **11**, 141 (1983).
[5] A. Howie and R. H. Milne, Ultramicroscopy **18**, 427 (1985).
[6] P. M. Echenique and J. B. Pendry, J. Phys. C **8**, 2936 (1975).
[7] P. M. Echenique, R. H. Ritchie, N. Barberán, and J. Inkson, Phys. Rev. B **23**, 6486 (1981).
[8] R. Garcia-Molina, A. Gras-Marti, A. Howie, and R. H. Ritchie, J. Phys. C **18**, 5335 (1985).
[9] R. H. Milne and P. M. Echenique, Solid State Commun. **55**, 909 (1985).
[10] F. Fujimoto and K. Komaki, J. Phys. Soc. Jpn. **25**, 1769 (1968).
[11] M. Schmeits, J. Phys. C **14**, 1203 (1981).
[12] H. Kohl, Ultramicroscopy **11**, 53 (1983).
[13] D. R. Penn and P. Apell, J. Phys. C **16**, 5729 (1983).
[14] T. L. Ferrell and P. M. Echenique, Phys. Rev. Lett. **55**, 1526 (1985).
[15] P. M. Echenique, Philos. Mag. B **52**, L9 (1985).
[16] R. Fuchs and F. Claro, Phys. Rev. B **35**, 3722 (1987).
[17] J. Bausells, A. Rivacoba, and P. M. Echenique, Surf. Sci. **189/190**, 1015 (1987).
[18] R. H. Ritchie, Philos. Mag. A **44**, 931 (1981).
[19] R. H. Ritchie and A. Howie, Philos. Mag. A **58**, 753 (1988).
[20] P. M. Echenique, J. Bausells, and A. Rivacoba, Phys. Rev. B **35**, 1521 (1987).
[21] Y. T. Chu, R. J. Warmack, R. H. Ritchie, W. Little, R. S. Becker, and T. L. Ferrell, Part. Accel. **16**, 13 (1984).
[22] D. De Zutter and D. De Vleeschauwer, J. Appl. Phys. **59**, 4146 (1986).
[23] C. A. Walsh, Philos. Mag. **59**, 227 (1989).
[24] N. Zabala, A. Rivacoba, and P. M. Echenique, Surf. Sci. **209**, 465 (1989).
[25] A. Rivacoba, P. Apell, and N. Zabala, Nucl. Instrum. Methods Phys. Res. Sect. B **96**, 465 (1995).
[26] B. L. Illman, V. E. Anderson, R. J. Warmack, and T. L. Ferrell, Phys. Rev. B **38**, 3045 (1988).
[27] R. Garcia-Molina, A. Gras-Marti, and R. H. Ritchie, Phys. Rev. B **31**, 121 (1985).
[28] D. Langbein, J. Phys. A **4**, 627 (1976).
[29] M. Schmeits and L. Dambly, Phys. Rev. B **44**, 12 706 (1991).
[30] M. Schmeits, Phys. Rev. B **39**, 7567 (1989).
[31] Z. L. Wang and J. M. Cowley, Ultramicroscopy **21**, 77 (1987); **21**, 335 (1987); **21**, 347 (1987); **23**, 97 (1987).
[32] N. Zabala and A. Rivacoba, Phys. Rev. B **48**, 14 534 (1993).
[33] P. E. Batson, Ultramicroscopy **9**, 227 (1982).
[34] P. E. Batson, Phys. Rev. Lett. **49**, 936 (1982).
[35] A. Howie and C. A. Walsh, Microsc. Microanal. **2**, 171 (1991).
[36] D. Ugarte, C. Colliex, and P. Trebbia, Phys. Rev. B **45**, 4332 (1992).
[37] F. Ouyang and M. Isaacson, Ultramicroscopy **31**, 345 (1989).
[38] F. Ouyang, P. E. Batson, and M. Isaacson, Phys. Rev. B **46**, 15 421 (1992).
[39] A. Liebsch, Phys. Rev. B **48**, 15 (1993).
[40] J. Tiggesbäumker, L. Köller, K. Meiwes-Broer, and A. Liebsch, Phys. Rev. A **48**, 1749 (1993).
[41] *Handbook of Optical Constants of Solids*, edited by E. D. Palik (Academic, London, 1985).
[42] I. S. Gradshteyn and I. M. Ryzhik, *Table of Integrals, Series and Products* (Academic, New York, 1980), p. 795.
[43] P. Morse and H. Feshbach, *Methods of Theoretical Physics* (McGraw-Hill, New York, 1953), pp. 745–748.
[44] A. Rivacoba, N. Zabala, and P. M. Echenique, Phys. Rev. Lett. **69**, 3362 (1992).
[45] E. Zaremba, Surf. Sci. **151**, 91 (1985).
[46] P. M. Echenique, A. Howie, and D. J. Wheatley, Philos. Mag. B **56**, 335 (1987).
[47] H. J. Hagemann, W. Gudat, and C. Kunz (unpublished).